J Therm Anal Calorim (2012) 109:227–235
DOI 10.1007/s10973-011-1714-3

Pyrolytic characteristics and kinetics of pistachio shell by thermogravimetric analysis

Korkut Açıkalın

Received: 26 April 2011 / Accepted: 26 May 2011 / Published online: 8 June 2011
© Akadémiai Kiadó, Budapest, Hungary 2011

Abstract Pyrolytic characteristics and kinetics of pistachio shell were studied using a thermogravimetric analyzer in 50–800 °C temperature range under nitrogen atmosphere at 2, 10, and 15 °C min^{-1} heating rates. Pyrolysis process was accomplished at four distinct stages which can mainly be attributed to removal of water, decomposition of hemicellulose, decomposition of cellulose, and decomposition of lignin, respectively. The activation energies, pre-exponential factors, and reaction orders of active pyrolysis stages were calculated by Arrhenius, Coats–Redfern, and Horowitz–Metzger model-fitting methods, while activation energies were additionaly determined by Flynn–Wall–Ozawa model-free method. Average activation energies of the second and third stages calculated from model-fitting methods were in the range of 121–187 and 320–353 kJ mol^{-1}, respectively. The FWO method yielded a compatible result (153 kJ mol^{-1}) for the second stage but a lower result (187 kJ mol^{-1}) for the third stage. The existence of kinetic compensation effect was evident.

Keywords Pistachio shell · Thermogravimetric analysis · Pyrolysis kinetics · Coats–Redfern method · Horowitz–Metzger method · Flynn–Wall–Ozawa method

Introduction

A great interest is focused on renewable energy sources since fossil fuels, the present major energy contributors, concern environmental problems, and show to be confronted with depletion in near future. Biomass is thought to be the most attractive renewable energy source owing to its availability, easy processability, and being environmentally friendly. It is already the fourth largest energy source in the world, and it is widely dispersed. Biomass materials, compared to coal, can be easily processed to produce chemicals and fuels since their reactivity and volatility are high [1]. Biomass materials capture the solar energy as fixed carbon via photosynthesis during which carbon dioxide is converted to organic compounds. Thus, their usage does not contribute to the increase of carbon dioxide concentration in the atmosphere [2]. The low sulfur and nitrogen contents of biomass materials (and derived fuels) cause less environmental pollution and health problems than fossil fuels when they are used in combustion processes [3]. It is also true that the usage of biomass waste materials as energy sources solves a part of waste disposal problems.

Biomass materials can also be used as raw materials to produce liquid, gaseous, and solid fuels unlike the other renewable energy sources. There are two main routes for this purpose: (i) biochemical conversion in which enzymatic activities takes place and (ii) thermochemical conversion in which biomass is exposed to heat or oxidation [4]. The main thermochemical conversion routes are pyrolysis, gasification, and liquefaction. Among these, pyrolysis is at spotlight since it enables to produce energy fuels at high fuel-to-feed ratios [5]. The biomass pyrolysis process can simply be described as the thermal decomposition of biomass at moderate temperatures (400–600 °C) in the absence of oxygen to obtain preferably liquid products (bio-oil) [6]. Pyrolysis is also involved in the combustion, gasification, and liquefaction processes of biomass as the initial step [7, 8]. Hence, knowledge of the characteristics and kinetics of pyrolysis step is vital to predict the behavior of biomass to design and control the necessary conversion units.

K. Açıkalın (✉)
Department of Chemical Engineering, Yıldız Technical University, 34210 Esenler, İstanbul, Turkey
e-mail: korkut.acikalin@gmail.com

Thermoanalytical techniques such as thermogravimetric analysis (TG) and derivative thermogravimetry (DTG) are commonly used to investigate the pyrolytic characteristics and kinetics of solid raw materials [9, 10]. In TG, the mass loss of a sample is measured against temperature under controlled heating rate and gas atmosphere, and then it is recorded in the form of TG curves. DTG curves are obtained by taking the first derivative of TG curves. It is known that kinetic parameters can be calculated from thermogravimetric curves since the shape of these curves is a function of reaction kinetics. For this purpose, several model-fitting (a reaction model has to be chosen) and model-free (does not require a reaction model) kinetic calculation methods were developed [11]. These calculation methods can follow either a differential or an integral approach to manipulate the TG data, and both have different disadvantages on which detailed information can be obtained from reference [12]. Arrhenius, Coats–Redfern, and Horowitz–Metzger methods are some examples for model-fitting kinetic calculation methods, and there are numerous studies available in literature as stated in references [13–15], [16–20], and [21, 22], respectively. The Flynn–Wall–Ozawa (FWO) method is one of the model-free isoconversional methods, and has been used in many studies [23–26].

This study aims to provide a clear understanding of the pyrolytic characteristics and kinetics of a biomass waste material, namely, pistachio shell. For this purpose, thermogravimetric analyses were performed at three different heating rates, and the related kinetic parameter values were calculated by Arrhenius, Coats–Redfern, Horowitz–Metzger, and FWO methods.

Materials and methods

Materials

In this study, the pyrolysis of pistachio shell was conducted by a thermogravimetric analyzer. Pistachios were obtained from a local market (Siirt, Turkey), and their shells were gently separated from the fruit. Shell samples were ground to particle size <0.1 mm using a Ika A11 model analytic mill. The samples were dried under vacuum at 105 °C, and kept in glass containers. The proximate and ultimate analyses data for pistachio shell are given in Table 1. Highly purified (99.99%, vol.) nitrogen was used as a carrier gas.

TG

The mass change of pistachio shell over the course of pyrolysis reaction was measured and recorded by Perkin Elmer Diamond TG/DTA system. The experiments were carried out non-isothermally at three different heating rates of 2, 10, and 15 °C min^{-1}. Nitrogen at a flowrate of 50 mL min^{-1} was used as a carrier gas. In each experiment, a sample mass of 8 ± 3 mg was used. The sample holders were open type platinum pans. The tests were conducted in the 50–800 °C temperature range.

Kinetic modeling

Biomass pyrolysis process may be represented by the following reaction scheme:

Biomass → Solid residue + Volatiles.

The fraction of pyrolyzed biomass (or conversion), α, is defined by the following expression:

$$\alpha = \frac{(m_0 - m_t)}{(m_0 - m_f)} \quad (1)$$

where m_0 is the mass of biomass at the beginning; m_t and m_f refer to the values at time t and at the end of the mass event of interest, respectively.

Pyrolysis rate, $d\alpha/dt$, is a linear function of temperature-dependent rate constant, k, and reaction model (a temperature-independent function of conversion), $f(\alpha)$:

$$\frac{d\alpha}{dt} = kf(\alpha). \quad (2)$$

Replacing the rate constant with Arrhenius equation, and introducing the heating rate ($\beta = dT/dt$) for non-isothermal case, Eq. 2 becomes:

$$\frac{d\alpha}{dt} = \frac{A}{\beta} e^{\left(-\frac{E}{RT}\right)} f(\alpha) \quad (3)$$

where A is the pre-exponential factor, E is the activation energy, R is the gas constant, and T is the absolute temperature.

Table 1 Proximate and ultimate analyses of pistachio shell

Proximate analysis/%					Ultimate analysis/%				
M[a]	VM[b,c]	FC[d,c]	Ash[c]	HHV[e]	C	H	O[f]	N	S
3.71	77.45	18.43	0.41	4155	44.62	5.81	49.25	0.32	–

[a] Moisture; [b] Volatile matter; [c] Calculated in dry basis; [d] Fixed carbon; [e] Higher heating value/kcal kg^{-1}; [f] Calculated by difference

Selecting *n*th order reaction model in the light of a previously accomplished kinetics study of pistachio shell in the literature [23], and rearranging, Eq. 3 becomes:

$$\frac{d\alpha}{(1-\alpha)^n} = \frac{A}{\beta} e^{\left(\frac{-E}{RT}\right)} dT. \quad (4)$$

In this study, Eq. 4 is the fundamental expression used in model-fitting kinetic calculation methods on the basis of TG data.

Results and discussion

Thermogravimetric analyses

TG/DTG curves

The TG and DTG curves for heating rates of 2, 10, and 15 °C min^{-1} are shown in Fig. 1. The whole pyrolysis process can be divided into four stages since every single slope change on a TG curve indicates the beginning of a new stage. By considering the TG/DTG curves obtained at 10 °C min^{-1}, the following observations and/or comments can be listed:

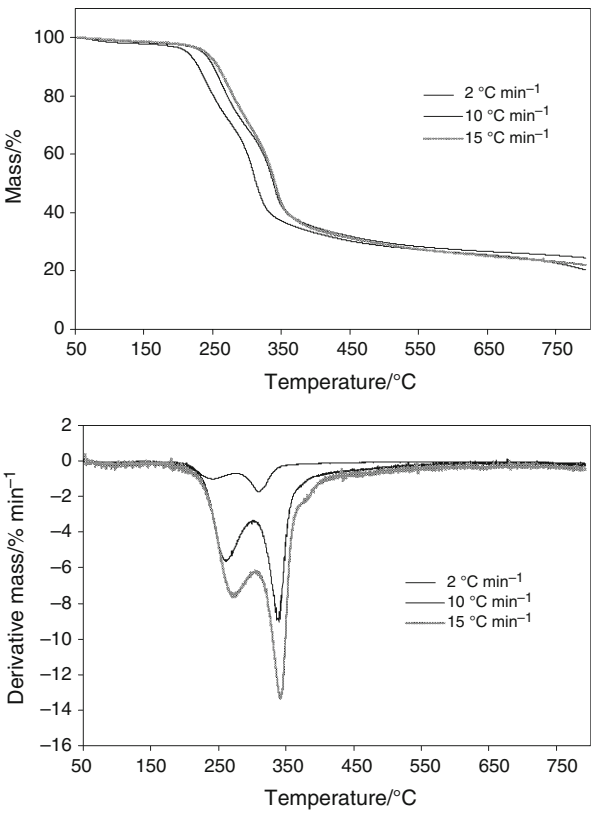

Fig. 1 TG (*upper*) and DTG curves of pistachio shell at different heating rates

(1) The first stage (stage I) starts at 50 °C and finishes at 222 °C. The mass loss occured in this stage was 3.33%, and can be attributed to the removal of water present in material and external water bounded by surface tension. It is also possible that some light volatile compounds are removed. Stage I is represented by the weak peak on the most left hand side of the DTG curve.

(2) The second stage (stage II), the upper "\"-shaped section on TG curve, starts at 222 °C and finishes at 298 °C with a mass loss of 26.99%. The corresponding area on the DTG curve is represented by the negative peak whose maximum is at 263 °C. The maximum mass loss rate was 5.59% min^{-1} at this stage. This stage can be referred as an active pyrolysis stage since mass loss rate is high.

(3) The third stage (stage III), the lower "\"-shaped section on TG curve, goes from 311 to 365 °C, and shows a mass loss of 26.73%. This stage is represented by the negative peak showing a maximum at 340 °C on the DTG curve. The maximum mass loss rate was 9.02% min^{-1} at this stage. This rate is also the maximum mass loss rate obtained during the whole pyrolysis process. This stage can also be referred as an active pyrolysis stage considering its high mass loss rate.

(4) The fourth stage (stage IV) starts at 365 °C and continues up to 800 °C, and it is seen as a tail in both TG and DTG curves. The mass loss occured in this stage was 14.17%. Stage IV can be referred as passive pyrolysis stage since mass loss rate is much lower compared to those in the second and third stages. The residual mass at the end of the overall pyrolysis process was determined as 24.53%.

(5) The mass losses observed in stage II, III, and IV can be explained by the components of pistachio shell. Pistachio shell is mainly composed of hemicellulose, cellulose, and lignin like all other lignocellulosic materials. The thermal degradation behavior of these components have been well studied, and it is known that hemicellulose, cellulose, and lignin complete their decompositions at temperature intervals of 210–325, 310–400, and 160–900 °C, respectively [27]. So, the mass losses of stage II, III, and IV can mainly be attributed to decomposition of hemicellulose, cellulose, and lignin, respectively.

(6) The ratios of hemicellulose, cellulose, and lignin in pistachio shell can not be determined exactly from TG/DTG curves since (i) the components decompose in overlapping temperature ranges and (ii) the components do not decompose completely but also form a residue. However, by combining the percentage values given above with the knowledge that lignin

yields ~40% of its mass as a residue at the end of the pyrolysis process, the lignin and holocellulose (hemicellulose + cellulose) ratios of pistachio shell can be estimated as 23.62 and 68.8%, respectively.

The effect of heating rate on pyrolysis characteristics

The characteristics related to active pyrolysis stages (stage II and stage III) such as starting temperature (T_i), ending temperature (T_f), maximum mass loss rate (W_{max}) and the temperature where this rate occured (T_{max}) were exactly determined for all studied heating rates, and their values are given in Table 2. It can be clearly said that all characteristic temperatures were shifted to higher values with increasing heating rate. This is because the heat transfer is not as effective and efficient as it was at lower heating rates. At lower heating rates, heating of biomass particles occurs more gradually leading to an improved and more effective heat transfer to the inner portions and among the particles [28]. The maximum mass loss rates were also shifted to higher temperatures with increasing heating rate as a consequence of the increasing effect of the inertia of the devolatilization process as the characteristic time of the process is decreased [29].

Calculation of kinetic parameter values

Model-fitting kinetic calculations

The reaction model describing the reaction mechanism is of high importance since the values of E and A depend on the assumed $f(\alpha)$. However, the pyrolysis of biomass includes complicated multiple reactions and thus, it is quite difficult to determine the reaction mechanism in needed detail to formulate the reaction kinetics. To overcome this situation, the process was simplified by lumping the complicated multiple reactions that takes place in carefully selected temperature ranges as an nth order reaction. The active pyrolysis stages (stage II and stage III), whose characteristics were explained thoroughly in previous section, were the temperature ranges subjected to kinetic calculations using Eq. 4. The kinetics of each stage was studied at 0.1–0.9 conversion interval to assure that linear parts of related stages on TG curve are at the focus of attention. The model-fitting kinetic calculation methods performed in this study were differential method of Arrhenius and integral methods of Coats–Redfern and Horowitz–Metzger.

The final rate equation of Arrhenius method can be obtained by taking the logarithm of Eq. 4 and making some rearrangements. It is given as follows:

$$\ln\left(\frac{d\alpha}{dT}\right) - n\ln(1-\alpha) = \ln\left(\frac{A}{\beta}\right) - \frac{E}{RT} \quad (5)$$

where

$$\frac{d\alpha}{dT} = \frac{\alpha_{T_2} - \alpha_{T_1}}{T_2 - T_1}. \quad (6)$$

According to Eq. 5, the plot of $\ln(d\alpha/dT) - n \ln(1 - \alpha)$ versus $(1/T)$ should give a straight line for the appropriate value of reaction order n. In order to determine the appropriate value of n for active pyrolysis stages, several values of n were chosen, the plots were drawn, and the related correlation coefficients (R^2) were calculated to generate R^2–n curves (Fig. 2a, b). Most appropriate n values ensuring the highest R^2 were determined from these curves for all studied heating rates. Using these values of n, final plots were drawn (Fig. 3a, b). The activation energy and pre-exponential factor of each active pyrolysis stages were calculated from the related slope ($-E$/R) and interception ($\ln(A/\beta)$) of final plots, respectively. The results obtained by Arrhenius method are given in Table 3. Note that kinetic parameters could not be calculated for the 2 °C min^{-1} heating rate since the generated plots were R^2–n lines instead of R^2–n curves. In other words, R^2 showed a continuous increase with selected n values.

In Coats–Redfern method, the integral of Eq. 4 is taken, and the resulting exponential integral which does not have an exact analytical solution is approximated using a Taylor

Table 2 Properties of active pyrolysis stages

Property	Heating rate/°C min^{-1}					
	2		10		15	
	S_{II}[a]	S_{III}[b]	S_{II}	S_{III}	S_{II}	S_{III}
T_i/°C	196	281	222	311	225	318
T_f/°C	269	340	298	365	299	371
T_{max}/°C	244	310	263	340	275	342
W_{max}/% min^{-1}	0.99	1.72	5.59	9.02	7.57	13.30

[a] Stage II; [b] Stage III

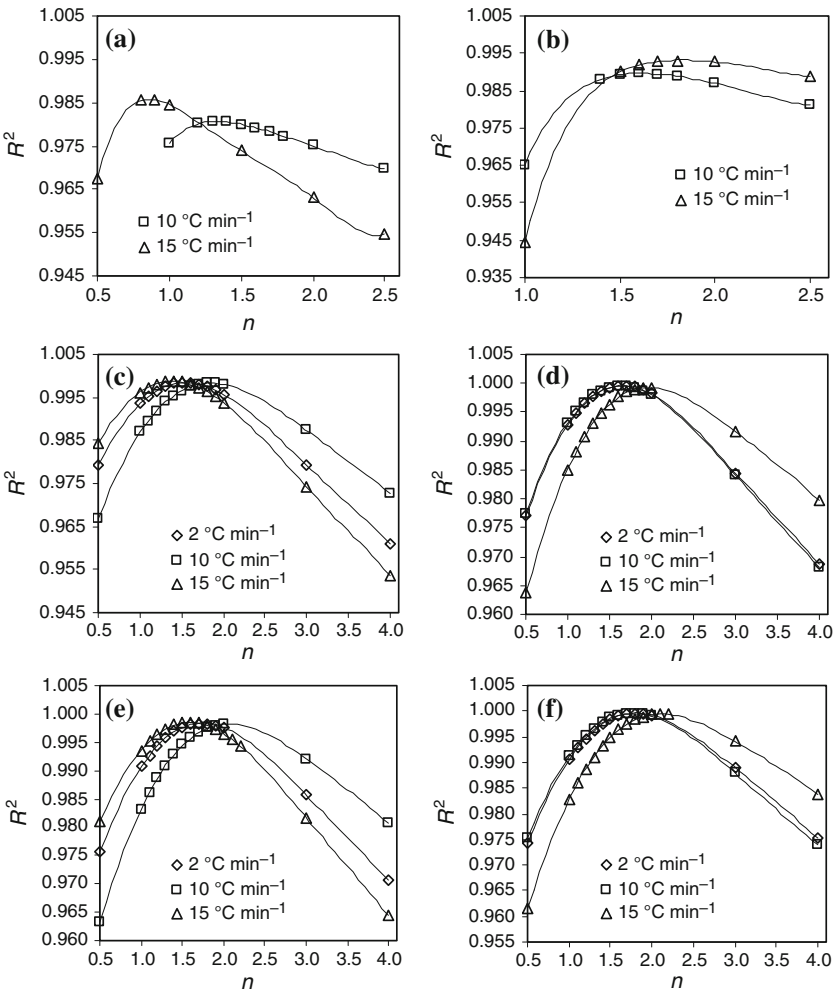

Fig. 2 R^2–n curves obtained by **a** Arrhenius method for stage II; **b** Arrhenius method for stage III; **c** Coats–Redfern method for stage II; **d** Coats–Redfern method for stage III; **e** Horowitz–Metzger method for stage II; and **f** Horowitz–Metzger method for stage III

series expansion. The obtained equation is simplified by considering $2RT/E \ll 1$. The final form is given as follows:

$$\ln g(\alpha) = -\frac{E}{RT} + \ln\left(\frac{AR}{\beta E}\right) \tag{7}$$

where $g(\alpha) = -(\ln(1-\alpha))/T^2$ if $n = 1$; $g(\alpha) = (1-(1-\alpha)^{(1-n)})/((1-n)T^2)$ if $n \neq 1$. In this method, a straight line should be obtained by plotting $\ln g(\alpha)$ versus $(1/T)$ if n is selected properly. So, R^2–n curves (Fig. 2c, d) were generated as explained in Arrhenius method, and the proper n values were determined for each active pyrolysis stage. Then, final plots (Fig. 3c, d) were drawn using these n values. The activation energy and pre-exponential factor of each active pyrolysis stage were determined from the slope $(-E/R)$ and the interception $(\ln((AR)/(\beta E)))$ of final plots, respectively. The results are given in Table 4.

In Horowitz–Metzger method, the linearized form of final equation is given as follows [30]:

$$\ln g(\alpha) = \left(\frac{E\Phi}{RT_{\max}^2}\right) + \ln\left(\frac{ART_{\max}^2}{\beta E}\right) - \frac{E}{RT_{\max}} \tag{8}$$

where $\Phi = T - T_{\max}$, and $T_{\max}$ is the temperature where maximum mass loss rate occurs. Here, $g(\alpha) = -\ln(1-\alpha)$ if $n = 1$; $g(\alpha) = (1-(1-\alpha)^{(1-n)})/(1-n)$ if $n \neq 1$. In this method, the appropriate reaction order is presumed to give the best linear plot of $\ln g(\alpha)$ versus Φ. The proper n values for each active pyrolysis stage were determined from R^2–n curves (Fig. 2e, f). Using these n values, final plots were drawn (Fig. 3e, f). The activation energy and pre-exponential factors were determined from slope $(E/(RT_{\max}^2))$ and intercept $(\ln((ART_{\max}^2)/(\beta E)) - E/(RT_{\max}))$, respectively. The results are shown in Table 5.

Model-free kinetic calculations

Isoconversional methods do not require knowledge of reaction mechanism to calculate activation energy. For this reason, they are referred as model-free methods. The FWO method is an integral isoconversional technique in which activation energy is related to heating rate and temperature at a constant conversion. The equation is as follows [8]:

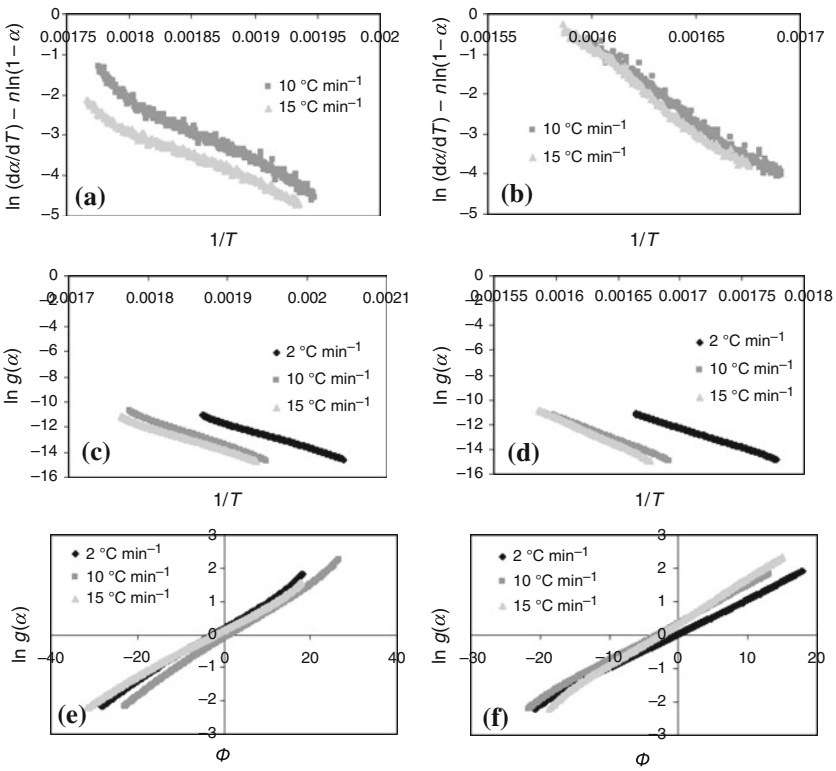

Fig. 3 Final plots obtained by **a** Arrhenius method for stage II; **b** Arrhenius method for stage III; **c** Coats–Redfern method for stage II; **d** Coats–Redfern method for stage III; **e** Horowitz–Metzger method for stage II; and **f** Horowitz–Metzger method for stage III

Table 3 Kinetic parameters calculated by Arrhenius method

B/°C min^{-1}	Stage	E/kJ mol^{-1}	Log A/min^{-1}	Plot equation	R^2	n
10	II	132.7	12.57	$y = -15959.2x + 26.65$	0.9806	1.32
	III	308.8	26.46	$y = -37133.7x + 58.62$	0.9896	1.61
15	II	109.4	10.22	$y = -13153.5x + 20.83$	0.9858	0.86
	III	339.8	29.20	$y = -40870.6x + 64.52$	0.9931	1.83
Average	II	121.1	11.40			1.09
	III	324.3	27.83			1.72

Table 4 Kinetic parameters calculated by Coats–Redfern method

B/°C min^{-1}	Stage	E/kJ mol^{-1}	Log A/min^{-1}	Plot equation	R^2	n
2	II	156.0	14.95	$y = -18765.8x + 23.88$	0.9985	1.55
	III	264.3	22.93	$y = -31782.9x + 41.73$	0.9997	1.64
10	II	180.3	17.35	$y = -21689.4x + 27.66$	0.9983	1.85
	III	321.0	27.49	$y = -38610.7x + 50.43$	0.9995	1.60
15	II	161.8	15.46	$y = -19461.0x + 23.01$	0.9990	1.52
	III	374.2	32.13	$y = -44999.6x + 60.55$	0.9993	1.90
Average	II	166.0	15.92			1.64
	III	319.8	27.52			1.71

$$\ln \beta = C_1 - \frac{E}{RT} \tag{9}$$

where C_1 is constant. According to Eq. 9, activation energy can be calculated from the slope of ln β versus $1/T$. Hence, the temperatures corresponding to the fixed values of conversion were measured at three different heating rates, and necessary plots were drawn (Fig. 4). Activation energy of active pyrolysis stages were calculated from the slopes ($-E/R$) of related plots at 0.1–0.9 conversion interval. The results are given in Table 6.

Table 5 Kinetic parameters calculated by Horowitz–Metzger method

B/°C min^{-1}	Stage	E/kJ mol^{-1}	Log A/min^{-1}	Plot equation	R^2	n
2	II	179.3	17.40	$y = 0.0806x + 0.196$	0.9983	1.75
	III	292.9	25.57	$y = 0.1036x + 0.039$	0.9996	1.82
10	II	200.9	19.43	$y = 0.0840x - 0.145$	0.9982	2.05
	III	353.8	30.36	$y = 0.1133x + 0.344$	0.9996	1.75
15	II	179.9	17.24	$y = 0.0720x + 0.146$	0.9985	1.58
	III	412.8	35.45	$y = 0.1311x + 0.378$	0.9994	2.09
Average	II	186.7	18.02			1.79
	III	353.2	30.46			1.89

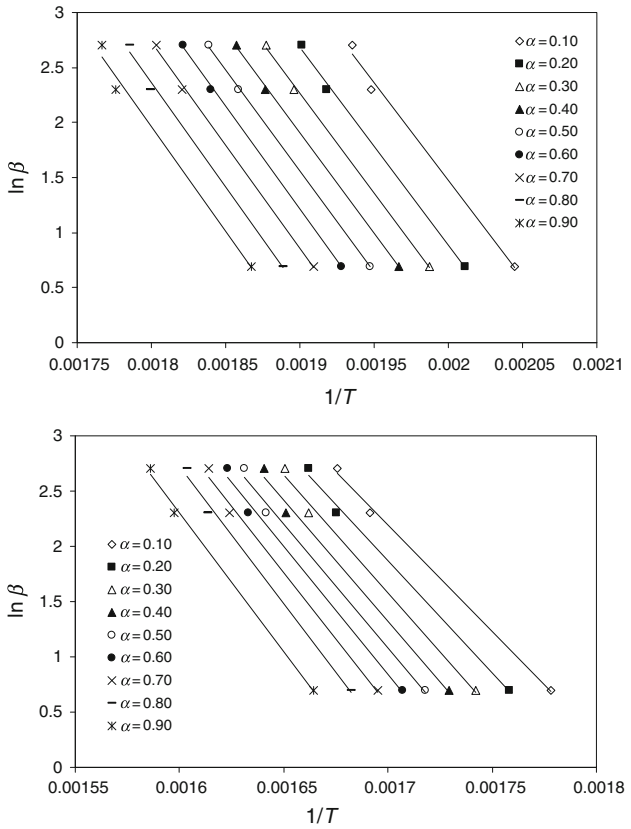

Fig. 4 Plots (*upper* for stage II; *lower* for stage III) obtained by FWO method for determination of activation energy

Evaluation of the calculated kinetic parameter values

Examining Tables 3, 4, and 5, it can be clearly said that heating rate has a great influence on activation energy. In active pyrolysis stages, the activation energy values calculated by all model-fitting kinetic calculation methods exhibited the same behavior with the changes in heating rate. In stage II, increasing heating rate from 2 to 10 °C min^{-1} resulted in an increase, but a further increase to 15 °C min^{-1} led to a decrease in activation energy values. On the other hand, in stage III, activation energy showed a continuous increase with increasing heating rate from 2 to 15 °C min^{-1}. Thus, it would be more righteous to compare the results on average basis (average of the results obtained at different heating rates). The average activation energy of stage II was calculated as 121.1, 166, and 186.7 kJ mol^{-1} by Arrhenius, Coats–Redfern, and Horowitz–Metzger methods, respectively. The model-free FWO method yielded 153 ± 5 kJ mol^{-1} in the 0.1–0.9 conversion interval which is compatible with the results given above but more closer to Coats–Redfern method result. For stage III, the average activation energy was calculated as 324.3, 319.8, and 353.2 by Arrhenius, Coats–Redfern and Horowitz–Metzger methods, respectively. The results are compatible but closer results were obtained by Arrhenius and Coats–Redfern methods. On the other hand, FWO yielded a considerably smaller result (184.5 ± 24 kJ mol^{-1}). This situation was also observed in Tonbul's study [23] on the pyrolysis of pistachio shell. He calculated the activation energy of stage II as 124–149 and 122-156 kJ mol^{-1} using Coats–Redfern and FWO methods, respectively. These results agree with this study. On the other hand for stage III, the values of 248–262 kJ mol^{-1} (obtained by Coats–Redfern method) and 146–181 kJ mol^{-1} (obtained by FWO method) were reported. There was an agreement with the results obtained by FWO method but for the Coats–Redfern

Table 6 Activation energies calculated by FWO method (kJ mol^{-1})

	Conversion degree/%									
	10	20	30	40	50	60	70	80	90	Avr.
Stage II	148	149	150	152	153	155	156	157	158	153
Stage III	160	169	176	182	187	192	199	205	209	187

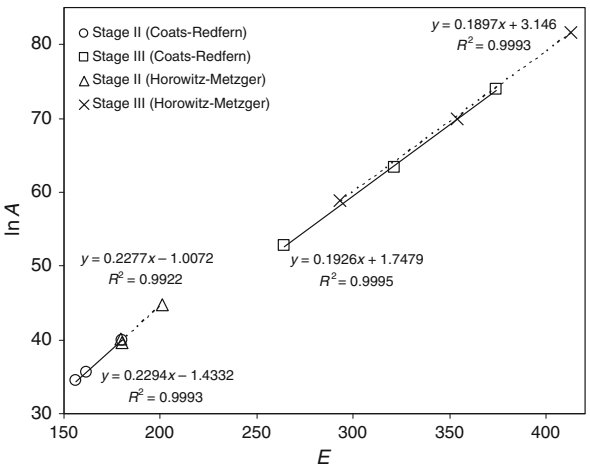

Fig. 5 Kinetic compensation effect

method the results of this study were higher than the reported values.

Generally speaking about both stages, Horowitz–Metzger method gave the highest results. This is an encountered occasion, and is generally attributed to the approximations of the method. The second fact observed from the studies was that the activation energy of stage III was always higher than the activation energy of stage II. This was an expected result since stage II and III represents the decomposition of hemicellulose and cellulose, respectively, and cellulose is known to be thermally more stable than hemicellulose. It was also observed that pre-exponential factor and activation energy exhibited the same behavior when the heating rate was changed. In other words, if activation energy decreases with a change in heating rate, pre-exponential factor decreases too, or vice versa. In literature, this situation is called as "kinetic compensation effect", and it is defined as "a rise in E (which will decrease the rate of reaction at any particular temperature) is partially or completely offset by an increase in A" [31]. In many cases, the variation of these parameters corresponds to the equation $\ln A = a + bE$, where a and b are constants [32]. So, ln A versus E plot was drawn (Fig. 5) to search for the existence of kinetic compensation effect. By considering the high correlation coefficient values shown in Fig. 5, the existence of kinetic compensation effect was confirmed.

Conclusions

Pyrolysis of pistachio shell has been carried out non-isothermally in the 50–800 °C temperature range at three different heating rates (2, 10, and 15 °C min^{-1}) under nitrogen atmosphere using a thermogravimetric analyzer.

(1) It was observed that ~65% pyrolysis conversion can be obtained at a relatively low temperature (~380 °C). This makes pistachio shell a potential raw material for pyrolysis process.

(2) TG/DTG curves indicated that pyrolysis process can be divided into four distinct stages which are mainly due to removal of water (stage I), decomposition of hemicellulose (stage II), decomposition of cellulose (stage III), and decomposition of lignin (stage IV), respectively. Most of the mass loss (~54%) was accomplished in stages II and III which were referred as active pyrolysis stages. The characteristic temperatures of these stages were shifted to higher values by increasing heating rate.

(3) The values of kinetic parameters related to active pyrolysis stages were calculated using various kinetic calculation methods. Their dependency on heating rate was clearly observed. For stage II, average E (kJ mol^{-1})–log A (min^{-1})–n values were calculated as 121.1-11.4-1.09, 166-15.92-1.64, and 186.7-18.02-1.79 from model-fitting kinetic calculation methods of Arrhenius, Coats–Redfern and Horowitz–Metzger, respectively. These values were calculated as 324.3-27.83-1.72, 319.8-27.52-1.71, and 353.2-30.46-1.89 for stage III. On the other hand, model-free FWO method yielded E values as 153 and 187 kJ mol^{-1} for stage II and stage III, respectively. So, it can be concluded that compatible results were obtained except Arrhenius "n" result in stage II and FWO "E" result in stage III.

(4) The existence of kinetic compensation effect was presented by establishing the functional relationship between activation energy and pre-exponential factor at different heating rates.

Acknowledgements The author would like to thank Işık Yavuz for her valuable help during the analyses. The author is also grateful to Dr. Dilek Duranoğlu and Prof. Dr. Esen Bolat for their continuous support throughout the study.

References

1. Naik S, Goud VV, Rout PK, Jacobson K, Dalai AK. Characterization of Canadian biomass for alternative renewable fuel. Renew Energy. 2010;35:1624–31.
2. Commandré JM, Lahmidi H, Salvador S, Dupassieux N. Pyrolysis of wood at high temperature: the influence of experimental parameters on gaseous products. Fuel Process Technol. 2010;92(5):837–44. doi:10.1016/j.fuproc.2010.07.009.
3. Isa KM, Daud S, Hamidin N, Ismail K, Saad SA, Kasim FH. Thermogravimetric analysis and the optimization of bio-oil yield from fixed-bed pyrolysis of rice husk using response surface methodology (RSM). Ind Crop Prod. 2011;33(2):481–7.
4. Valden MV, Baeyens J, Brems A, Janssens B, Dewil R. Fundamentals, kinetics and endothermicity of the biomass pyrolysis reaction. Renew Energy. 2010;35:232–42.

5. Shuping Z, Yulong W, Mingde Y, Chun L, Junmao T. Pyrolysis characteristics and kinetics of the marine microalge *Dunaliella tertiolecta* using thermogravimetric analyzer. Bioresour Technol. 2010;101:359–65.
6. Mohan D, Pittman CU, Steele PH. Pyrolysis of wood/biomass for bio-oil: a critical review. Energy Fuels. 2006;20:848–89.
7. Wang Z, Cao J, Wang J. Pyrolytic characteristics of pine wood in a slowly heating and gas sweeping fixed-bed reactor. J Anal Appl Pyrolysis. 2009;84:179–84.
8. Hu S, Jess A, Xu M. Kinetic study of Chinese biomass slow pyrolysis: comparison of different kinetic models. Fuel. 2007; 86:2778–88.
9. Aboulkas A, El harfi K, El bouadili A, Nadifiyine M, Benchanaa M, Mokhlisse A. Pyrolysis kinetics of olive residue/plastic mixtures by non-isothermal thermogravimetry. Fuel Process Technol. 2009;90:722–8.
10. Yang Q, Wu S, Lou R, Lv G. Analysis of wheat straw lignin by thermogravimetry and pyrolysis-gas chromatography/mass spectrometry. J Anal Appl Pyrolysis. 2010;87:65–9.
11. Cabrales L, Abidi N. On the thermal degradation of cellulose in cotton fibers. J Therm Anal Calorim. 2010;102(2):485–91.
12. White JE, Catallo WJ, Legendre BL. Biomass pyrolysis kinetics: a comparative critical review with relevant agricultural residue case studies. J Anal Appl Pyrolysis. 2011;91(1):1–33.
13. Sheeba KN, Babu JSC, Jaisankar S. The reaction kinetics for coir pith pyrolysis in the thermogravimetric analyzer. Energy Sour. Part A. 2010;32(19):1837–50.
14. Munir S, Daood SS, Nimmo W, Cunliffe AM, Gibbs BM. Thermal analysis and devolatilization kinetics of cotton stalk, sugar cane bagasse and shea meal under nitrogen and air atmospheres. Bioresour Technol. 2009;100:1413–8.
15. Syed S, Quadaih R, Talab I, Janajreh I. Kinetics of pyrolysis and combustion of oil shale sample from thermogravimetric data. Fuel. 2011;90(4):1631–7.
16. Lu C, Song W, Lin W. Kinetics of biomass catalytic pyrolysis. Biotechnol Adv. 2009;27:583–7.
17. Haykiri-Acma H, Yaman S. Thermal reactivity of rapeseed (*Brassica napus* L.) under different gas atmospheres. Bioresour Technol. 2008;99:237–42.
18. Hui Z, Huaxiao Y, Mengmeng Z, Song Q. Pyrolysis characteristics and kinetics of macroalgae biomass using thermogravimetric analyzer. Proc World Acad Sci Eng Technol. 2010;65: 1161–6.
19. Lou R, Wu S-B. Pyrolysis characteristics of rice straw emal. Cellul Chem Technol. 2008;42(7–8):371–80.
20. Wang S, Jiang XM, Wang N, Yu LJ, Li Z, He PM. Research on pyrolysis characteristics of seaweed. Energy Fuels. 2007;21(6): 3723–9.
21. Slovák V, Šušák P. Pitch pyrolysis kinetics from single TG curve. J Anal Appl Pyrolysis. 2004;72:249–52.
22. Vijayakumar CT, Vinayagamoorthi S, Fink JK, Sivasamy P. Characterization of low rank alpine coals: thermogravimetric studies. J Anal Appl Pyrolysis. 2006;76:191–7.
23. Tonbul Y. Pyrolysis of pistachio shell as a biomass. J Therm Anal Calorim. 2008;91(2):641–7.
24. Zhao Y, Bie R, Lu J, Xiu T. Kinetic study on pyrolysis of NSSC black liquor in a nitrogen atmosphere. Chem Eng Commun. 2010;197(7):1033–47.
25. Li D, Chen L, Zhang X, Ye N, Xing F. Pyrolytic characteristics and kinetic studies of three kinds of red algae. Biomass Bioenergy. 2011;35(5):165–77.
26. Li D, Chen L, Yi X, Zhang X, Ye N. Pyrolytic characteristics and kinetics of two brown algae and sodium alginate. Bioresour Technol. 2010;101:7131–6.
27. Açıkalın K. Thermogravimetric analysis of walnut shell as pyrolysis feedstock. J Therm Anal Calorim. 2010. doi:10.1007/s10973-010-1267-x.
28. Idris SS, Rahman NA, Ismail K, Alias AB, Rashid ZA, Aris MJ. Investigation on thermochemical behaviour of low rank Malaysian coal, oil palm biomass and their blends during pyrolysis via thermogravimetric analysis (TGA). Bioresour Technol. 2010; 101:4584–92.
29. Lapuerta M, Hernández JJ, Rodríguez J. Kinetics of devolatilisation of forestry wastes from thermogravimetric analysis. Biomass Bioenergy. 2004;27:385–91.
30. Janković B, Adnadević B, Jovanović J. Non-isothermal kinetics of dehydration of equilibrium swollen poly(acrylic acid) hydrogel. J Therm Anal Calorim. 2005;82:7–13.
31. L'vov BV. Thermal decomposition of solids and melts: new thermochemical approach to the mechanism, kinetics and methodology. Berlin: Springer; 2007.
32. Rodríguez RP, Sierens R, Verhelst S. Thermal and kinetic evaluation of biodiesel derived from soybean oil and higuereta oil. J Therm Anal Calorim. 2009;96(3):897–901.